



Surface plasmon-polariton resonances and optical rectification in finite gratingsP. Moroshkin ^{1,*}, J. Plumitallo,¹ T. Ochiai ², R. Osgood, III,³ and Jimmy Xu^{1,4}¹*School of Engineering, Brown University, Providence, Rhode Island 02912, USA*²*Research Center for Electronic and Optical Materials, National Institute for Materials Science, Tsukuba 305-0044, Japan*³*Army DEVCOM SC, Natick, Massachusetts 01760, USA*⁴*Department of Physics, Brown University, Providence, Rhode Island 02912, USA*

(Received 13 June 2023; accepted 11 September 2023; published 25 September 2023)

The optical rectification effect is observed in periodically structured metal films (metasurfaces) with broken inversion symmetry. It is found that the finite width of the metasurface and the proximity of its edges also provide a symmetry-breaking mechanism, adding to the rectification current, which is further enhanced at surface plasmon polariton resonances. By position- and angle-resolved measurements we show that this mechanism is more efficient than the symmetry breaking achieved either by the oblique incidence of the laser light or by a nonsymmetric structure of the unit cell. The existing theory of the optical rectification can partially account for the observed phenomena.

DOI: [10.1103/PhysRevA.108.033519](https://doi.org/10.1103/PhysRevA.108.033519)**I. INTRODUCTION**

Optical rectification (OR) refers to a nonlinear optical process generating a dc electric current or voltage in a sample irradiated with light. In metal films, the effect is due to the momentum transfer from light to free electrons and is therefore frequently termed a photon drag [1–4]. Excitation of surface plasmon polariton (SPP) resonances at the surface of a metal film greatly increases the local oscillating electric field and the electron density oscillations and therefore leads to the enhancement of the optical rectification current [5–8].

In order to transform symmetric oscillations of free electrons driven by the incident light wave into a direct current, the system must break the inversion symmetry along the direction of the photocurrent. This is usually achieved by the oblique incidence of the laser beam onto the metal surface (film). At normal incidence, optical rectification can be obtained in structured metal films, where the inversion symmetry is broken by the structure. For example, periodic one-dimensional (1D) gratings and two-dimensional (2D) nanohole arrays with broken inversion symmetry of a unit cell were used in Refs. [6,8–11] to demonstrate optical rectification current at a normal incidence.

Theoretically, the OR effect in the presence of SPP waves was analyzed within the framework of the electron hydrodynamic model, taking into account a particular grating structure [5,11,12]. The calculations in general agree with the trends observed in the experimental data, although the actual magnitude of the photocurrent remains difficult to predict. In some cases, the experimentally observed current exceeds the theoretical result by an order of magnitude. The authors attribute the discrepancy to the poorly known effect of the metal surface roughness and other nonidealities.

In the present work we address another aspect of OR experiments that is usually not treated by the theory. Typically, the

photocurrent is measured in periodic metal gratings with the area of $\lesssim 1 \text{ mm}^2$, consisting of several hundreds of unit cells. The laser beam may cover only a part of the grating and/or overlap some of the grating edges, thus producing additional symmetry breaking. However, the overlap between the laser spot and the grating area in most cases is not well documented, making it difficult to decipher its impact or contribution. At the same time, the theory is always formulated assuming periodic boundary conditions, i.e., it only applies for infinite planar structures with a strict periodicity and no boundaries.

The excitation of surface plasmon polaritons on finite-size gratings has been addressed in a number of experimental and theoretical studies [13–17]. It was demonstrated that a very small number (less than ten) of unit cells is sufficient for an efficient coupling of the incident light and the SPP waves [13,14,18].

Below, we present the measurements of the OR effect, with precise control of the overlap between the laser spot and the grating, with the laser beam focused off-center of the grating. We compare our experimental results with the predictions of the most up-to-date theoretical model [12] for infinite grating. We then modify the model and carry out a series of calculations for a finite-size grating with the same unit cell dimensions. By comparing the experimental and calculated OR signals, we identify a previously unknown contribution to the OR effect that is enhanced by the excitation of SPP resonances, but has a polarity determined by the off-center position of the laser spot. This new mechanism thus can only be obtained in a finite periodic grating.

II. EXPERIMENT**A. Experimental setup**

Our experimental setup is similar to that described in our earlier publications [11,19]. Photocurrent is measured in a 1D grating shown in Fig. 1. It consists of rectangular ridges or terraces made of gold and placed on top of a continuous gold film on a glass substrate. The grating consists of

*petr_moroshkin@brown.edu

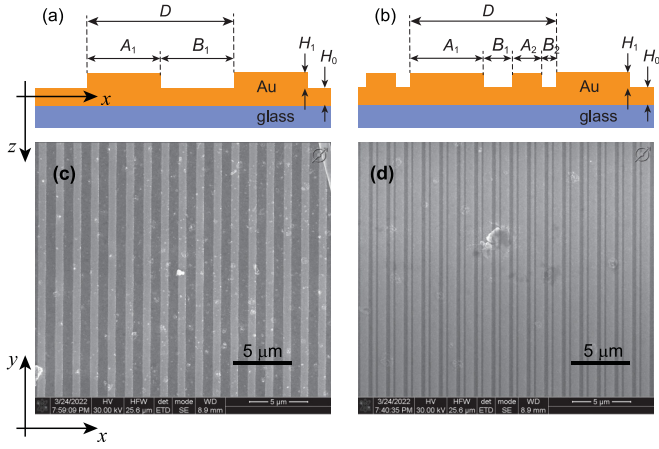


FIG. 1. (a) and (b) Sketches and (c) and (d) SEM images of 1D gratings used in the experiment. (a) and (c) show the symmetric profile of a unit cell, and (b) and (d) show the asymmetric profile.

450 unit cells with a period $D = 1488$ nm and has a transversal width $d = 200$ μm . The terraces have a height $H_1 = 60$ nm and the underlying continuous metal film has a thickness $H_0 = 100$ nm.

Structures with two different unit cell profiles were investigated. The unit cell profile shown in Fig. 1(a) possesses inversion symmetry. It consists of a single terrace (ridge) and a groove designed with the widths $A_1 = B_1 = D/2$. According to the scanning electron microscope (SEM) image of Fig. 1(c), the actual terrace width is $A_1 = 640$ nm.

The grating of the second type is shown in Figs. 1(b) and 1(d). It has the same period D , film thickness H_0 , and terrace height H_1 , but the unit cell is designed to break the inversion symmetry. The unit cell consists of two terraces of unequal widths: A_1 and A_2 separated by grooves with the widths B_1 and B_2 . According to the design, $A_1 = D/2$, $A_2 = B_1 = D/5$, and $B_2 = D/10$. It thus differs from the symmetric structure only by the second terrace A_2 added to the unit cell.

This design, also used in Refs. [8,9,11], ensures a broken inversion symmetry of the unit cell that is essential for the optical rectification (photon drag) effect. It was demonstrated [8,9,11] to generate a significant unidirectional photocurrent even under a normal incidence of the laser beam, in a purely symmetric experimental configuration. An SEM image of the grating is shown in Fig. 1(d). The measurements show the actual dimensions of the unit cell as $A_1 = 640$ nm, $A_2 = 200$ nm, $B_1 = 400$ nm, and $B_2 = 250$ nm.

The gratings of both types were prepared by a sequence of steps including optical lithography and gold film deposition to form a 5×0.2 mm stripe of continuous gold film, with electric contacts on both ends. The grating, with the grooves and ridges orthogonal to the long axis of the stripe, is fabricated in the second layer of gold film deposited on top of the first one, by applying e-beam lithography and a lift-off process. The resulting samples have the electric resistance of 10–12 Ω .

The setup is shown in Fig. 2(a). The sample is illuminated by a cw solid-state laser at the wavelength $\lambda_{\text{Las}} = 808$ nm, with the power of 100 mW. The laser is on-off modulated at a frequency of ~ 100 Hz with a mechanical chopper. In the present experiment, the grating is oriented with the grooves

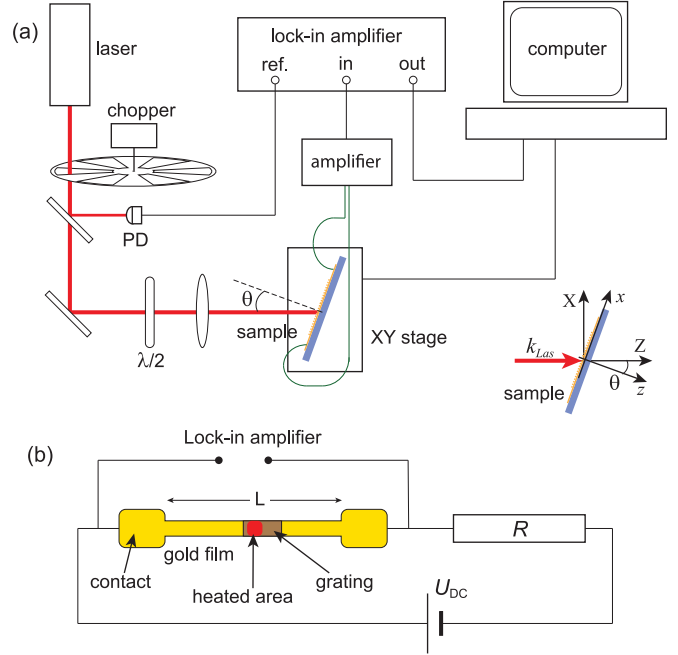


FIG. 2. (a) Experimental setup used in the OR measurements. The inset shows the orientation of the coordinate axes of the laboratory frame (X, Z) and of the sample frame (x, z). PD: photodiode, $\lambda/2$: half-wave plate. (b) Sketch of the sample and the circuit used for the resistivity measurements. $R = 1$ k Ω , $U_{DC} = 20$ V, $L = 5$ mm.

and ridges parallel to the Y axis (vertical) and the photocurrent is measured along the metal film stripe underneath and orthogonal to the grooves. The laser beam is incident on the grating along the Z axis and the sample normal lies in the XZ plane, at the angle θ with respect to the laser beam. The laser is linearly polarized along the X axis (P polarization), orthogonally to the grooves of the grating.

The laser beam is focused to a spot with a diameter of ~ 100 μm that can be centered anywhere within the sample area. This is achieved by translating the sample in the xy plane orthogonal to the incident laser beam with a computer-controlled motor-driven translation stage. Typically, we record either 1D scans in the x direction (orthogonal to the grooves) or 2D XY maps by translating the sample in steps of 10 or 20 μm . At each step, the signal of interest (see below) is measured with the help of a lock-in amplifier and stored in the computer.

In order to characterize the optical and electric response of each grating, two types of measurements were carried out. The optical rectification current was amplified by a transimpedance current to voltage amplifier with a low input resistance (< 1 Ω) and an output gain of 10^5 V/A. The amplified voltage signal was detected by a lock-in amplifier, referenced at the chopper frequency.

The second measurement is required in order to determine the absorbance of the grating that varies both with the angle of incidence and the position of the laser spot on the sample. The absorbed laser light leads to the heating of the gold film and thus locally increases its electric resistance:

$$R_{\text{film}}(T) = R_{\text{film}}(T_0) \left(1 + \sigma \Delta T \frac{\Delta L}{L} \right) \quad (1)$$

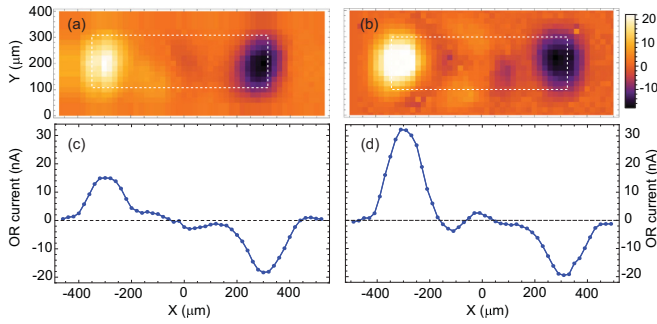


FIG. 3. (a) and (b) Experimental 2D maps of optical rectification current. (c) and (d) Plots of the OR current vs the laser spot X . $P_{\text{Las}} = 100$ mW, normal incidence, laser spot diameter FWHM = $110 \mu\text{m}$, dashed white rectangles show the grating contours. (a) and (c) show symmetric grating, while (b) and (d) show nonsymmetric grating.

Here, T is the absolute temperature of the heated part of the film, $T_0 = 293$ K, $\Delta T = T - T_0$, and $\sigma = 3.4 \times 10^{-3} \text{ K}^{-1}$ is the temperature coefficient of resistivity of gold. For simplicity, it is assumed that the heated area has the same width d ($=200 \mu\text{m}$) as the gold stripe on which the grating is placed and its length ΔL is equal to its width. $L = 5$ mm is the total length of the gold film stripe, excluding the contacts, much longer than the grating.

For the resistance measurement, a circuit shown in Fig. 2(b) was used. A dc current of 20 mA is passed through the sample and a $R = 1 \text{ k}\Omega$ resistor connected in series. The voltage drop on the gold film is measured by the same lock-in amplifier, referenced at the chopper frequency.

$$U_{\text{lockin}} = I_{\text{dc}} R_{\text{film}}(T_0) \frac{\Delta L}{L} \sigma \Delta T \quad (2)$$

The method provides an absolute measurement of the time-varying film conductivity and temperature that is directly proportional to the absorbed laser power and thus to the sample absorbance. Typically, an oscillating voltage signal with the amplitude of $\sim 50 \mu\text{V}$ was measured, corresponding to the time-dependent local temperature increase $\Delta T \approx 1.5$ K. Under the same conditions, laser illumination of the gold film outside of the patterned area (grating) produced a temperature increase of the order of 0.2 K.

B. Optical rectification and absorption at normal incidence

A typical 2D map of the OR current excited in a symmetric grating under normal incidence is shown in Fig. 3(a). A corresponding X -scan of the OR signal [i.e., a horizontal cut through Fig. 3(a)] is shown in Fig. 3(c). In theory (of an infinite grating), this grating is expected to produce zero OR signal at normal incidence. This is indeed the case when the laser beam is focused in the middle of the grating. Nevertheless, one can clearly see two symmetric regions near the left and right edges of the grating that produce a strong OR current of the opposite polarities. The OR current reaches ~ 20 nA. Its dependence on X is antisymmetric, with a zero crossing at the center of the grating.

Figure 4(a) shows a map of the absorbed laser power (heating) in the same symmetric grating, under the same experimental conditions. A horizontal cut through this 2D map

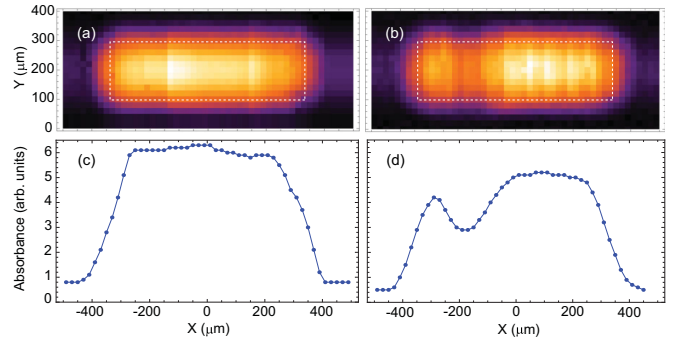


FIG. 4. (a) and (b) Experimental 2D maps of optical absorbance by the gratings visualized via the heating effect. (c) and (d) Plots of the laser heating effect vs the laser spot X . $P_{\text{Las}} = 100$ mW, normal incidence, laser spot diameter FWHM = $110 \mu\text{m}$, dashed white rectangles show the grating contours. (a) and (c) show symmetric grating, while (b) and (d) show nonsymmetric grating.

is shown in Fig. 4(c). The figure shows approximately uniform absorbance over the entire grating area.

The observation of a relatively uniform absorbance in the entire grating area together with the SEM images of the sample (Fig. 1) demonstrate the homogeneity and the absence of large defects in the grating structure. It allows us to rule out the possibility that the OR current shown in Fig. 3 originates from the grating inhomogeneity or is induced by some thermal mechanism.

We have repeated the same set of measurements on the sample with a nonsymmetric unit cell, as shown in Fig. 1(b). The resulting XY maps of the OR current and laser-induced heating are shown in Figs. 3(b) and 4(b), respectively. The corresponding X -scans of both the OR current and heating are plotted in Figs. 3(d) and 4(d), respectively. Both 2D maps are qualitatively very similar to those obtained with symmetric grating. The OR current is maximized (~ 30 nA) with the laser focused near the left and right edges of the grating, with the opposite polarities. Besides these two main maxima near the grating edges, in Figs. 3(b) and 3(d) one can see a rather complex dependence of the OR current on both X and Y coordinates in the central part of the grating. These secondary structures have a much smaller magnitude, ~ 1 – 5 nA. At present we cannot reliably attribute them either to the defects of the sample or to some other mechanism induced by the nonsymmetric structure of the unit cell.

In Figs. 4(b) and 4(d), the spatial variation of the heating-induced resistive change signal in the middle of the grating is slightly larger than that observed in the symmetric grating. This variation is not reproduced in different samples and is therefore attributed to the film nonuniformity, or defects.

C. Angle of incidence dependence

Varying the incidence angle in the range $-50^\circ < \theta < +50^\circ$ does not change the characteristic structure of the XY OR maps shown in Fig. 3. Although the grating slightly shifts, depending on the incidence angle, due to an inevitable slight spatial mismatch between the vertical rotation axis and the center of the grating, the distance between the positive and negative OR maxima remains constant in the coordinate frame

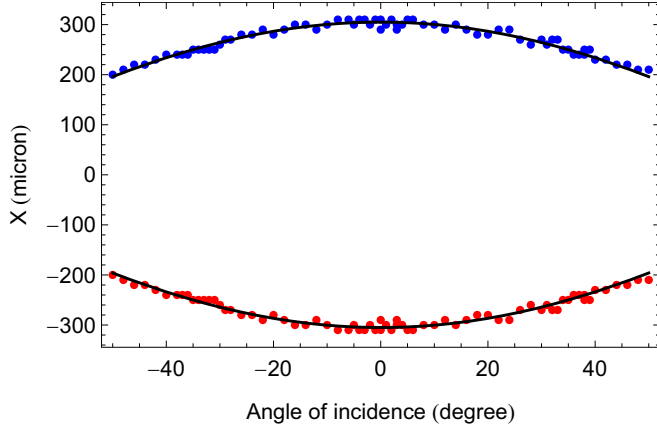


FIG. 5. X coordinates of the positive and negative OR maxima plotted vs the angle of incidence. Dots indicate experimental data, solid lines are from Eq. (3). Nonsymmetric grating.

of the sample. The two OR maxima are observed at the positions of the translation stage that we denote X_1 and X_2 , respectively, and the center of the grating is at X_0 . After subtracting the shift of the grating center, $X_1(\theta)$ and $X_2(\theta)$ are plotted in Fig. 5. Under the oblique incidence, the two coordinates follow the projection of the grating onto the plane orthogonal to the laser beam simply because the grating is rotated in the laboratory frame,

$$X_{1,2}(\theta) = X_0 \mp B \cos \theta. \quad (3)$$

By fitting the experimental data with Eq. (3), we determine $2B = 610 \mu\text{m}$, $60 \mu\text{m}$ less than the width of the grating.

The structure of the heating maps (Fig. 4) remains unchanged with the laser incidence angle varied in the range of $-50^\circ < \theta < +50^\circ$. The width of the heated area also follows the dependence $\propto \cos \theta$, corresponding to the projection of the grating width onto the X axis.

Figure 6(a) shows the measured OR current signal in the symmetric grating, as a function of the angle of incidence θ . For each value of θ , the laser spot was moved across the entire grating in the X direction in $20 \mu\text{m}$ steps, with the OR current measured at each step. The red and blue curves shown in the figure represent the data taken with the laser beam focused on the right and the left sides of the grating, respectively, corresponding to the two main maxima of Fig. 3(c). Note that the two currents have opposite polarities, and their absolute values are plotted in the figure.

The angular dependence of the laser-induced heating for the same symmetric grating is plotted in Fig. 6(b). In the same figure we show a plot of the grating absorbance numerically computed with the help of the COMSOL model. The details of this calculation are given below, in Sec. III A. The experimental curve is shown on arbitrary vertical scale, adjusted to match the computed curve.

The angular dependence of the OR current is very similar to that of the experimentally measured laser heating effect. Both plots closely follow the theoretically calculated absorbance curve. There are six peaks observed at $\theta = \pm 3^\circ, \pm 30^\circ$, and $\pm 37^\circ$. These peaks are assigned to six SPP

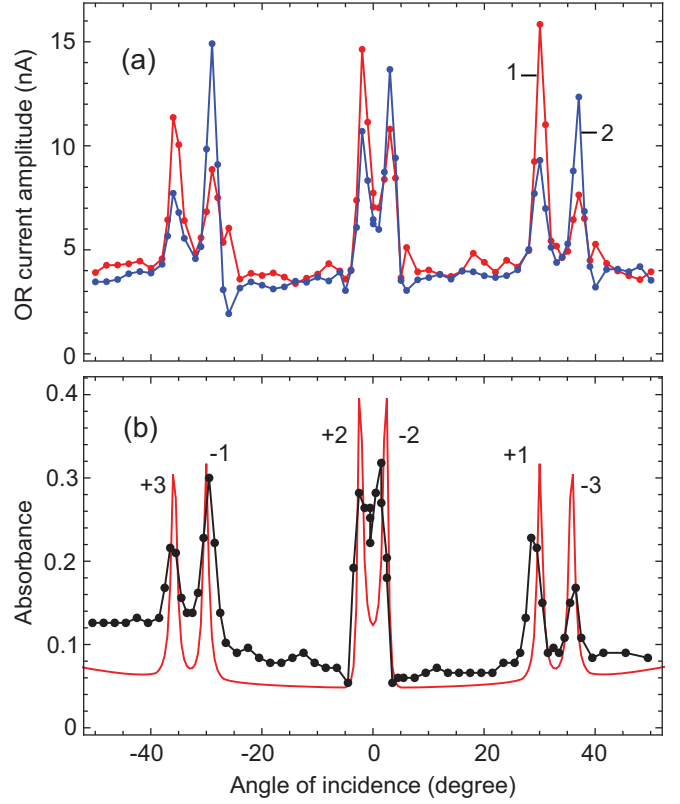


FIG. 6. Dependencies on the angle of incidence, symmetric grating. (a) Experimental OR current magnitude: blue line and dots indicate the left edge of the grating, red line and dots indicate the right edge of the grating. (b) Grating absorbance: black line and dots show the experimental signal (heating) plotted on an arbitrary scale, red line is the absorbance calculated with COMSOL. SPP resonances are labeled with the corresponding m indices according to Eq. (4).

resonances of the grating. Their resonant θ angles can be estimated by the momentum-conservation equation:

$$K_{\text{SPP}}(\omega_{\text{Las}}) = |k_{\text{Las}} \sin \theta + mq| \quad (4)$$

Here, $K_{\text{SPP}}(\omega_{\text{Las}})$ is the wave vector of SPP at the laser frequency, $k_{\text{Las}} = 2\pi/\lambda_{\text{Las}}$ is the laser wave vector, and $q = 2\pi/D$ is the grating “crystal momentum.” We approximate the wave vector of the SPP in the grating as close to that in an unstructured gold film:

$$K_{\text{SPP}}(\omega_{\text{Las}}) \approx k_{\text{Las}} \sqrt{\frac{\varepsilon_g}{\varepsilon_g + 1}}, \quad (5)$$

where $\varepsilon_g(\omega)$ is the dielectric susceptibility of gold [20].

The resonances at $\theta = \pm 3^\circ$ fulfill Eq. (4) with $m = \mp 2$, resonances at $\theta = \pm 30^\circ$ correspond to $m = \pm 1$, and resonances at $\theta = \pm 37^\circ$ - to $m = \mp 3$, respectively. The discrepancy between the calculated and measured resonance angles θ_m does not exceed 2° . Each resonance is labeled in Fig. 6(b) with the corresponding m index.

Most important, the OR current excited on either the left or right side of the grating does not change its sign (polarity), when the angle of incidence is changed from $\theta > 0$ to $\theta < 0$. As discussed below, theoretical models [5,7,12] considering

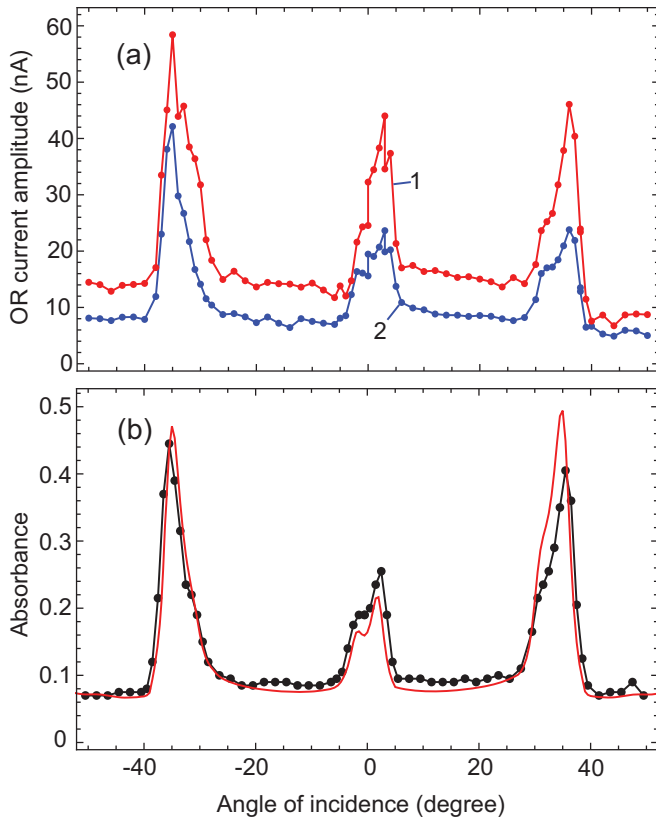


FIG. 7. Dependencies on the angle of incidence, nonsymmetric grating. (a) Experimental OR current magnitude: blue line and dots indicate the left edge of the grating, red line and dots indicate the right edge of the grating. (b) Grating absorbance: black line and dots show the experimental signal (heating) plotted on an arbitrary scale, red line is the absorbance calculated with COMSOL.

infinite periodic sample structures lead to antisymmetric dependencies of the OR current on the angle of incidence. The same can be expected by applying a most general symmetry argument, at least for a symmetric grating structure.

The angular dependence of the experimental OR current, measured from the left and right sides of the nonsymmetric grating are plotted in Fig. 7(a). The corresponding plots of the laser-induced heating and of the computed absorbance are shown in Fig. 7(b). All four plots share the same characteristic structure. However, in contrast to the symmetric grating (Fig. 6), there are only three relatively broad and asymmetric peaks centered at $\theta \approx 0, \pm 35^\circ$. The two grating structures studied in the present experiment have the same period $D = 1488$ nm. Equation (4) therefore predicts exactly the same set of θ values for the resonant excitation of various SPP modes. However, in the nonsymmetric grating the three closely spaced pairs of resonances $m = \pm 2, m = +3, -1$, and $m = -3, +1$ become unresolved.

Again, as in the case of the symmetric grating, the OR current from either side of the grating does not change its sign when the incidence angle is changed from positive to negative. OR signals obtained from a nonsymmetric grating of a very similar design were reported in our earlier

publication [8]. In that experiment, the gratings had a smaller area, $150 \times 100 \mu\text{m}$, and a slightly larger height of the terraces, $H_1 = 80$ nm. The grating period and the structure of the unit cell were the same as shown in Fig. 1(a), with two terraces per unit cell.

In that experiment we have obtained a maximum OR current of 4 nA, significantly smaller than in the present work. The difference is due to a much larger input resistance of the current measurement apparatus ($1 \text{ k}\Omega$) that was used in Ref. [8]. At the same time, the angular dependence of the OR current reported in Ref. [8] closely corresponds to that shown in Fig. 7(a).

Figure 3 demonstrates that OR currents in our samples are generated predominantly near the grating edges. At the same time, the presence of the prominent SPP resonance peaks in the OR signals in Figs. 6 and 7 proves that the OR current originates from the periodic structures of both gratings and not at the edges themselves.

III. THEORETICAL MODEL

A. Optical rectification in an infinite grating

The absorption and diffraction of light by 1D gold gratings were calculated with the help of a finite-element solver COMSOL MULTIPHYSICS. We have studied the gratings with two different structures of the unit cell corresponding to those shown in Figs. 1(a) and 1(b): symmetric and nonsymmetric, respectively. In the calculation, we introduce a finite steepness of the groove or ridge sides $s = |\partial z / \partial x|$ varied in the range of 10–40. This range is consistent with the terrace edges being sharper than the resolution of our experimental SEM images of Fig. 1. $D = 1488$ nm, $\lambda_{\text{Las}} = 808$ nm. Here, we use a coordinate system (x, y, z) connected with the sample, as shown in Fig. 1 and in the inset of Fig. 2(a). A frequency-domain analysis is performed in a 2D geometry corresponding to the xz plane, with perfectly matched layers placed above and below the grating to avoid non-physical reflections. Periodic Floquet boundary conditions are imposed at $x = 0$ and $x = D$, corresponding to an infinitely broad grating, uniformly illuminated by an infinite plane wave.

The resulting absorbance curves for the gratings of both types are shown in Figs. 6(b) and 7(b) and are in good agreement with the experimental data.

The calculations also provide electric field distributions in the gold film and above it. As expected, the locally enhanced electric field is mostly concentrated near the corners of the terraces forming the grating, similar to our earlier calculations [8]. The knowledge of the local E-field distribution allows us to apply the theory of optical rectification effect developed by Kurosawa *et al.* [12]. Their model considers a sample (film) characterized by a complex Drude polarizability $\alpha(\omega) = \alpha_R(\omega) + i\alpha_I(\omega)$ and a cross-sectional area $A_x(x)$, periodically modulated along the x direction. By applying a hydrodynamic model of the electron motion, the authors of Ref. [12] arrive at the following expression for the voltage generated across the sample in the x direction due to the

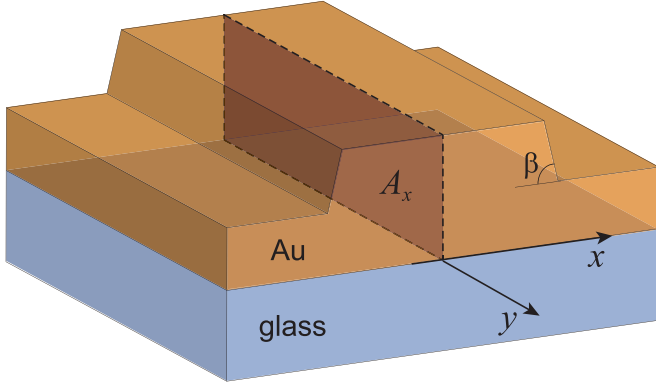


FIG. 8. A sketch of the grating terrace illustrating the slope of terrace edge $s = \tan \beta$ and the film cross section $A_x(x)$.

photon drag effect:

$$\begin{aligned}
 U_X = & \frac{1}{\rho} \int \frac{dx}{A_x(x)} \left[\int dA_x \left(\frac{\alpha_R(\omega)}{4} \nabla |\mathbf{E}|^2 \right. \right. \\
 & + \frac{\alpha_I(\omega)}{2} \text{Im}\{E_j^* \nabla E_j\} - \frac{\gamma}{2\omega} \text{Im}\{\nabla \cdot (\mathbf{P} \otimes \mathbf{E})\} \\
 & + b \frac{\gamma}{2\omega} \text{Im}\{P_{\perp}(x^-) E_{\parallel}(x^-)^*\} \hat{\mathbf{t}}(x) \cdot \hat{\mathbf{x}} \\
 & \left. \left. + \frac{|\alpha|}{4} |E_{\perp}(x^-)|^2 \hat{\mathbf{n}}(x) \cdot \hat{\mathbf{x}} \right] \right]. \quad (6)
 \end{aligned}$$

Here, we follow the notations of Ref. [12]. \mathbf{E} and \mathbf{P} are complex vectors of electric field amplitude and induced polarization of the material, and E_j represents E_x , E_y , and E_z components. ρ is the electron charge density, γ is a phenomenological damping factor of the electron motion, and b represents surface diffusion and scattering effects near the metal surface. The last two terms involve electric field and polarization at the surface of the metal, denoted $E_{\parallel,\perp}(x^-)$ and $P_{\perp}(x^-)$, respectively. $\hat{\mathbf{n}}$ and $\hat{\mathbf{t}}$ are surface normal and tangential unit vectors, respectively, and $\hat{\mathbf{x}}$ is a unit vector in the x direction.

The general expression (6) is then simplified [12] by assuming $\alpha_I \ll |\alpha_R|$ and $\gamma \ll \omega$ and neglecting the terms proportional to α_I and γ/ω ,

$$\begin{aligned}
 U_X = & \frac{1}{\rho} \int dx \left[\frac{\alpha_R}{4} \langle |\mathbf{E}(\mathbf{r})|^2 \rangle_{A_x} \frac{1}{A_x} \frac{\partial A_x}{\partial x} \right. \\
 & \left. + \frac{|\alpha|}{4} \langle |E_{\perp}(x^-)|^2 \rangle_{A_x} \hat{\mathbf{n}}(x) \cdot \hat{\mathbf{x}} \right]. \quad (7)
 \end{aligned}$$

Here, the expressions $\langle |\mathbf{E}(\mathbf{r})|^2 \rangle_{A_x}$ and $\langle |E_{\perp}(x^-)|^2 \rangle_{A_x}$ represent the averaged values of $|\mathbf{E}(\mathbf{r})|^2$ and $|E_{\perp}(x^-)|^2$ over the surface A_x .

A sketch of one grating terrace with a highlighted cross section A_x is shown in Fig. 8. The quantities $\partial A_x/\partial x$ and $\hat{\mathbf{n}}(x) \cdot \hat{\mathbf{x}}$ are zero everywhere except the steep edges of the terraces (grooves). The OR voltage is thus generated at these edges, where the transversal film cross section is changing abruptly and where the surface normal is nearly parallel to

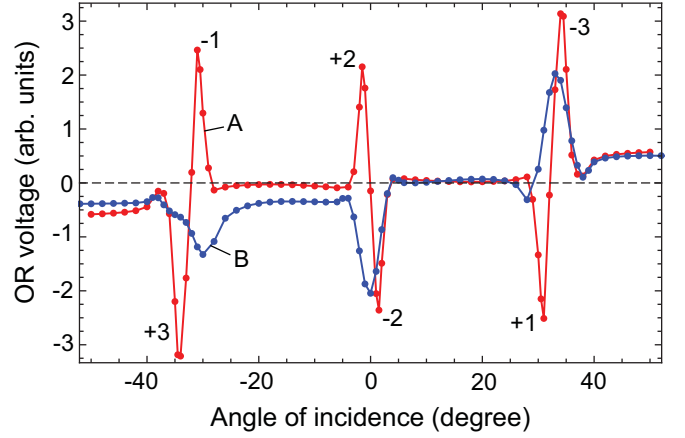


FIG. 9. OR voltage computed according to Eq. (7) for an infinite periodic grating, as a function of the angle of incidence. Curve A (red) is symmetric grating, curve B (blue) is nonsymmetric grating. SPP resonances are labeled with the corresponding m indices, as in Fig. 6.

the x axis. Note that the contributions of the opposite sides of the same groove or terrace have different signs and therefore would compensate each other in the absence of symmetry breaking.

We replace the integral in Eq. (7) by a summation over the edges of the terraces in the unit cell, multiplied by the number of the unit cells in the sample. At the edges of the terraces,

$$\frac{1}{A_x} \frac{\partial A_x}{\partial x} = \pm \frac{s}{H_0 + s\delta x}. \quad (8)$$

And the electric field is taken from the electric field maps calculated with COMSOL.

The results of the calculation are plotted vs the angle of incidence in Fig. 9. The experimentally investigated OR current is expected to be proportional to U_X , with the proportionality constant depending on the geometric parameters of the sample, contact resistance, and input impedance of the measuring electronics. In addition, the magnitude of the calculated OR voltage depends on the steepness of the terraces and on the number of unit cells illuminated by the laser. Here, we do not attempt any quantitative comparison between the experimental and theoretical OR signals and therefore plot the computed U_X on the arbitrary scale, the same for both gratings.

For both grating structures, the calculated $U_X(\theta)$ shows the same SPP resonance peaks as the corresponding absorbance curves in Figs. 6(b) and 7(b). This confirms the conclusions of Refs. [8,12,21,22] that the OR effect is greatly enhanced by the excitation of SPP resonances due to the intensification of the local electric field. The pairs of resonances $m = -2, +2$, $m = +3, -1$, and $m = -3, +1$ for the nonsymmetric grating are unresolved, as they are in the corresponding absorbance curve and in the experimental data.

In agreement with the symmetry arguments, the θ dependence of OR from the symmetric grating is perfectly antisymmetric, with a zero crossing at $\theta = 0$. On the other hand, for the nonsymmetric grating the angular dependence is neither symmetric nor antisymmetric, with a strong OR current excited at $\theta = 0$.

The main discrepancy between the computed (Fig. 9) and experimentally measured (Figs. 6 and 7) OR signals is in the polarity of the SPP resonance peaks. For the symmetric grating, the SPP resonances $m = +3, -2, +1$ have the opposite polarity of the resonances $m = -1, +2, -3$. For the nonsymmetric grating, the polarity of the peak at $\theta = +33^\circ$ corresponding to the superposition of $m = +1$ and $m = -3$ resonances is opposite that of two other peaks. The model is also unable to account for the dependence of the OR current on the position of the laser spot within the grating and the proximity to the grating edge. We therefore conclude that the finite size of the grating plays an essential role in the experimentally observed OR effect.

Variation of the edge steepness s does not lead to qualitative changes in the dependence of $U_X(\theta)$. At $s = 10$ the second (surface) term in Eq. (7) dominates. At a larger steepness, $s = 40$, the first (bulk) term becomes dominant. However, both of them have similar dependences on θ . Since we are aiming at the qualitative description of the OR mechanism, in the calculations presented below, the steepness was kept constant.

B. Optical rectification in a finite grating

We have modified our COMSOL model to compute the electric field profiles of a finite grating without imposing a periodic boundary condition. The model grating size is kept within a realistic range of computational demand. The one presented here consists of 20 symmetric unit cells with a profile identical to that analyzed above and shown in Fig. 1(a). On both sides of the grating having the length $L_G = 19.5 \times D = 29 \mu\text{m}$ (between the left edge of the first terrace and the right edge of the 20th terrace), the model includes a flat gold film with a thickness of 100 nm and a length of 20 μm . The incident laser beam has a Gaussian transversal profile with a full width at half maximum (FWHM) diameter $w_0 = 5 \mu\text{m}$, centered at $x = 0$. The laser spot thus is significantly smaller than the grating area, as it is in the experiment. The center of the grating is at $x = X_0$ that is shifted with respect to the center of the laser spot. $X_0 = -14.5 \mu\text{m}$ correspond to the laser spot centered at the right edge of the grating and $X_0 = +14.5 \mu\text{m}$ to that at the left edge, as shown in Fig. 10.

Typical 2D maps of the electric field amplitude are shown in Fig. 10. In this figure one can clearly see the incident and diffracted laser light and the SPP waves propagating along the grating and the metal film on both sides of it. No SPP can be seen in Fig. 10(a), since the laser spot has no overlap with the grating. The three maps in Figs. 10(b)–10(d) show the laser beam incident on the grating at $\theta = 0$, where two overlapping SPP resonances, $m = -2, +2$ are excited, with the two corresponding SPP waves propagating in the opposite directions. As shown in Fig. 10(b), with the laser spot centered at the right edge of the grating, the $m = +2$ SPP wave propagating to the right from the grating is significantly stronger than the $m = -2$ wave to the left. The situation is reversed in Fig. 10(d), with the laser spot on the left edge of the grating. Similar behavior can be seen also in the vicinity of other SPP resonances at $-40^\circ < \theta < -25^\circ$ and $+40^\circ > \theta > +25^\circ$.

We then apply Eq. (7) [12] to calculate the voltage generated by this finite grating. The summation is made over

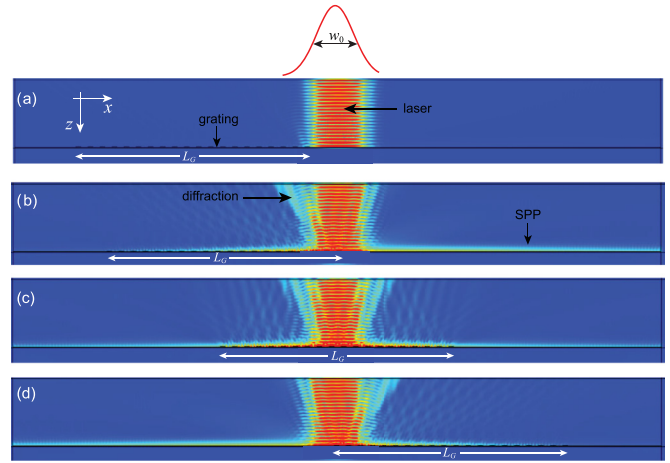


FIG. 10. Computed 2D maps of the electric field amplitude produced by laser illumination of a finite symmetric grating. Normal incidence. Laser spot is positioned (a) outside of the grating ($X_0 = -18 \mu\text{m}$), (b) at the right edge of the grating ($X_0 = -14.5 \mu\text{m}$), (c) at the grating center ($X_0 = 0$), and (d) at the left edge of the grating ($X_0 = +14.5 \mu\text{m}$). White horizontal line shows the grating width L_G . Upper panel shows the transversal profile of the incident laser beam.

the edges of all 20 terraces forming the grating. The region outside the grating does not contribute to the voltage in Eq. (7) due to $\partial A_x / \partial x = 0$ and $(\hat{\mathbf{n}}(x) \cdot \hat{\mathbf{x}}) = 0$.

The computed U_X vs X_0 dependence is shown in Fig. 11. At normal incidence, $\theta = 0$, the $U_X(X_0)$ curve is antisymmetric with respect to the $X_0 = 0$, when the laser spot is centered at the grating center. The situation at $\theta = 0, X_0 = 0$ is equivalent to the infinite periodic grating, with the OR voltage equal to zero due to the grating symmetry. However, when the laser spot is positioned off-center with respect to the grating, still at normal incidence, a significant nonzero OR voltage is generated. Its polarity is determined by the sign of X_0 . The positive and negative voltage maxima correspond to the laser spot centered at $X_0 = +11 \mu\text{m}$ and $-11 \mu\text{m}$, approximately

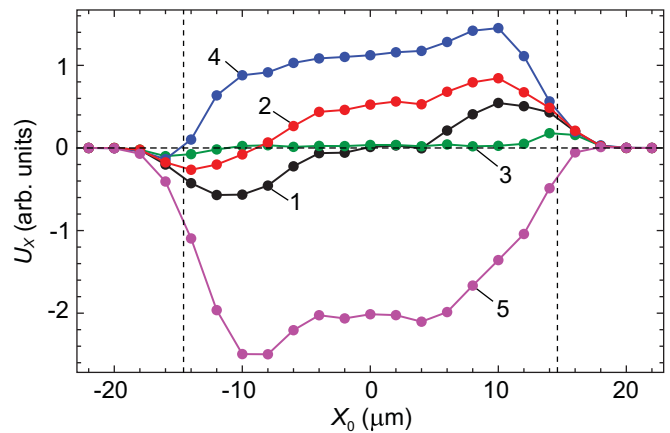


FIG. 11. Computed OR voltage U_x in a finite symmetric grating vs X_0 . Curve 1 (black): $\theta = 0$, curve 2 (red): $\theta = -2^\circ$, curve 3 (green): $\theta = -20^\circ$, curve 4 (blue): $\theta = -29^\circ$, curve 5 (magenta): $\theta = -34^\circ$. Vertical dashed lines show the edges of the grating at $X_0 = 0$.

3 μm away from the left and right grating edge, respectively. This distance is of the same order as the laser spot radius, similar to the experimental observations. Shifting the laser spot further off-center leads to a decrease of the laser power incident on the grating and thus to a decrease in the OR effect.

The other curves in Fig. 11 show the U_X vs X_0 dependence at different angles of incidence θ . Under $\theta \neq 0$ the dependence is not antisymmetric any more. Exciting the SPP resonances at $\theta = \pm 2^\circ$, $\pm 29^\circ$, and $\pm 34^\circ$ leads to the enhancement of OR voltage, with the entire grating generating either positive or negative U_X , in agreement with the angular dependence for the infinite grating shown in Fig. 9. On the other hand, at $\theta = \pm 20^\circ$, we obtain a much weaker, nonresonant OR effect that can be seen only with the laser beam centered exactly at the grating edges, at $X_0 = \pm 14.5 \mu\text{m}$.

The complex behavior of the OR voltage in Fig. 11 can be interpreted as a competition of three mechanisms: (1) resonant SPP-enhanced OR effect that is best captured by the model of Kurosawa *et al.* for the infinite grating; (2) nonresonant OR effect at the edges of the grating, weakly dependent on the angle of incidence; and (3) another mechanism that is most efficient when the pump laser is focused somewhere between the center and the edge of the grating. The latter effect seems to be dominant in our experimental data. Its characteristic feature is the antisymmetric dependence on X_0 , with the left and right sides of the grating generating the OR signals of the opposite polarities.

Under the excitation of the SPP resonances, the theoretical model of Ref. [12] predicts the OR signal dominated by the “standard” mechanism, the same as for the infinite grating. Only at $\theta = 0$, when the “standard” OR effect is zero, the new bipolar off-center OR effect can be clearly seen. Note also a negative feature in the $\theta = -34^\circ$ curve at $X_0 = -10 \mu\text{m}$ and a positive bump in the $\theta = -2^\circ$ and $\theta = -29^\circ$ curves at $X_0 = +10 \mu\text{m}$. They probably result from the interference between mechanisms (1) and (3) under the SPP resonance conditions.

As a possible mechanism of the OR enhancement near the grating edge we consider the reflection of the laser-excited SPP wave at the edge. The interference of the laser-induced SPP wave with the same wave reflected at the grating edge may lead to the enhancement of the local electric field and thus amplify the OR current. This interference will be localized in close proximity of the edge due to a short coherence length of the SPP waves. The SPP propagating in the opposite

direction has to travel a much larger distance before reaching the other edge of the grating and thus loses its coherence. These qualitative considerations are not fully included in the simple numerical model neglecting decoherence, so that no significant OR enhancement near the grating edges can be seen in Fig. 11. Furthermore, it remains unclear why the experimentally observed OR current at each edge keeps its polarity independent of the incidence angle reversal of the laser beam. Further research is needed in order to elucidate the observed effects.

IV. CONCLUSIONS

We have studied the OR effect in a 1D plasmonic grating, with special attention on the finite-size effects arising due to the off-center position of the laser-illuminated spot with respect to the grating. Previous studies have assumed infinitely large, uniformly illuminated gratings and thus neglected an important symmetry-breaking mechanism produced by the off-center (nonuniform) illumination. In agreement with earlier studies, our experiment has demonstrated the OR effect that is enhanced by the resonant excitation of the SPP waves in the periodically structured metal film. The magnitude of the observed OR current in a nonsymmetric grating is a factor of four larger than that in a symmetric grating, under the same experimental conditions. Its dependence on the angle of incidence varies with the unit cell structure in the same way as the grating absorbance.

In contrast to earlier studies, the polarity of the generated OR current in our experiment is entirely controlled by the off-center position of the laser-illuminated spot with respect to the grating center and the edges. The same dependence is observed in both symmetric and nonsymmetric grating structures, in the entire range of the incidence angle studied in this work. The existing theory of the OR effect in periodic plasmonic structures, modified for the finite size of the grating, only partially accounts for the experimentally observed effect.

ACKNOWLEDGMENTS

This exploration was supported in part by AFOSR (Grant No. FA 9550-19-1-0355), ARO (Grant No. W911NF211081), by Army DEVCOM SC (Grant No. W911QY2220004), and by JSPS KAKENHI (Grant No. 22K03488).

-
- [1] J. E. Goff and W. L. Schaich, *Phys. Rev. B* **56**, 15421 (1997).
 - [2] M. Akbari, M. Onoda, and T. Ishihara, *Opt. Express* **23**, 823 (2015).
 - [3] G. M. Mikheev, A. S. Saushin, V. V. Vanyukov, K. G. Mikheev, and Y. P. Svirko, *Nanoscale Res. Lett.* **12**, 39 (2017).
 - [4] J. H. Strait, G. Holland, W. Zhu, C. Zhang, B. R. Ilic, A. Agrawal, D. Pacifici, and H. J. Lezec, *Phys. Rev. Lett.* **123**, 053903 (2019).
 - [5] A. English, C. W. Cheng, L. Lowe, M. H. Shih, and W. Kuang, *Appl. Phys. Lett.* **98**, 191113 (2011).
 - [6] H. Kurosawa, T. Ishihara, N. Ikeda, D. Tsuya, M. Ochiai, and Y. Sugimoto, *Opt. Lett.* **37**, 2793 (2012).
 - [7] M. Durach and N. Noginova, *Phys. Rev. B* **93**, 161406(R) (2016).
 - [8] P. Moroshkin, T. Ochiai, R. Osgood, and J. Xu, *AIP Adv.* **11**, 115006 (2021).
 - [9] T. Hatano, B. Nishikawa, M. Iwanaga, and T. Ishihara, *Opt. Express* **16**, 8236 (2008).
 - [10] M. Akbari, J. Gao, and X. Yang, *Appl. Phys. Lett.* **114**, 171102 (2019).
 - [11] P. Moroshkin, J. Plumitallo, T. Ochiai, R. Osgood, and J. M. Xu, *Phys. Rev. A* **106**, 023521 (2022).
 - [12] H. Kurosawa, S. Ohno, and K. Nakayama, *Phys. Rev. A* **95**, 033844 (2017).

- [13] I. P. Radko, S. I. Bozhevolnyi, G. Brucoli, L. Martin-Moreno, F. J. Garcia-Vidal, and A. Boltasseva, *Phys. Rev. B* **78**, 115115 (2008).
- [14] G. Leveque and O. J. F. Martin, *J. Appl. Phys.* **100**, 124301 (2006).
- [15] A. Baron, E. Devaux, J. C. Rodier, J. P. Hugonin, E. Rousseau, C. Genet, T. W. Ebbesen, and P. Lalanne, *Nano Lett.* **11**, 4207 (2011).
- [16] G. Li, F. Xiao, L. Cai, K. Alameh, and A. Xu, *New J. Phys.* **13**, 073045 (2011).
- [17] C. Chen and P. Berini, *Opt. Express* **18**, 8006 (2010).
- [18] D. Benner, J. Boneberg, P. Nürnberger, R. Waitz, P. Leiderer, and E. Scheer, *Nano Lett.* **14**, 5218 (2014).
- [19] P. Moroshkin, M. J. Yu, and J. Xu, *Phys. Rev. A* **107**, 033504 (2023).
- [20] A. D. Rakic, A. B. Djurisic, J. M. Elazar, and M. L. Majewsky, *Appl. Opt.* **37**, 5271 (1998).
- [21] N. Noginova, A. V. Yakim, J. Soimo, L. Gu, and M. A. Noginov, *Phys. Rev. B* **84**, 035447 (2011).
- [22] N. Noginova, V. Rono, F. J. Bezares, and J. D. Caldwell, *New J. Phys.* **15**, 113061 (2013).